INVERSION OF TWO-DIMENSIONAL SPHEROIDAL PARTICLE DISTRIBUTIONS FROM BACKSCATTER, EXTINCTION AND DEPOLARIZATION PROFILES VIA REGULARIZATION

Christine Böckmann and L. Osterloh

Universität Potsdam, Institut für Mathematik, Am Neuen Palais 10, 14469 Potsdam, Germany, Email: bockmann@uni-potsdam.de

ABSTRACT

We consider an ensemble of spheroidal particles characterized by the complex refractive index, the aspect ratio and the size parameter of volume equivalent spheres, i.e., the aspect ratio is the additional microphysical parameter which goes beyond the conventional Mie theory. We propose a two-dimensional (2D) model to retrieve spheroidal particle distributions, depending not only on the size parameter but also on the aspect ratio, and microphysical particle properties from Raman lidar and depolarization profiles in contrast to conventional procedures. Since the problem is ill-posed in nature we use an appropriate iterative regularization technique to retrieve the 2D particle distribution.

1. INTRODUCTION

Studying the influence of non-spherical cloud and aerosol particles on the radiation budget of Earth's atmosphere is of growing importance in remote sensing. Polar stratospheric clouds and Cirrus clouds, for example, may contain large populations of non-spherical ice crystals which have a major impact on how those clouds scatter radiation. Saharan dust storms as well as volcanic eruptions are other sources of non-spherical aerosol particles which are important for a better understanding of the direct and indirect climate effects of such global events. There exist essential differences in the light scattering behavior between spherical and non-spherical particles. We can observe an increasing side scattering behavior and the appearance of a backscattering depolarization if non-spherical particles are considered, see e.g. [1] and [2]. Such spheroidal particles are used as microphysical models in recent measurement campaigns like AERONET, EARLINET, and SAMUM to study the effect of non-spherical particles on different measurement scenarios and to estimate their influence on the radiative forcing, see e.g. [3, 4, 5, 6]. We investigated the role that depolarization profiles play in this inversion process to retrieve the particle distribution.

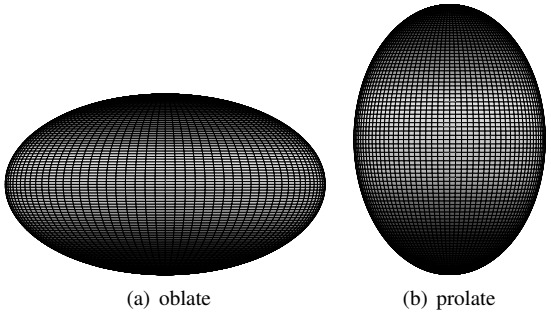

(a) oblate (b) prolate

Figure 1: Two spheroids. On the left, an oblate spheroid with $a = 0.5$, on the right, a prolate spheroid with $a = 1.5$.

2. SPHEROIDAL PARTICLES

Let us denote by $r_{\rm v}$ the vertical semi-axis (rotating axis) of a spheroid and by $r_{\rm h}$ the horizontal one. This means for the aspect ratio $a = r_{\rm v}/r_{\rm h}$. A spheroid is created by rotating the curve defined by

$$r(\vartheta) = r_{\rm v}\left(\sin^2\vartheta + \frac{r_{\rm h}^2}{r_{\rm v}^2}\cos^2\vartheta\right)^{-1/2}, \quad \vartheta \in [0, 2\pi). \tag{1}$$

See Fig. 1 for examples of oblate and prolate spheroids.

The inversion will be performed with the following data $\Gamma_j,\ j \in \{\text{bsca}, \text{hv}, \text{ext}\}$: the total particle backscatter at 355, 532 and 1064 nm and cross-polarization component of particle backscatter at 355, 532 and 1064 nm as well as particle extinction coefficients at 355 and 532 nm (3bsca+3hv+2ext wavelengths λ). Since we will assume r to denote the radius of the volume equivalent sphere, the volume distribution $v(r, a) = \frac{4\pi r^3}{3} n(r, a)$ is basically still valid by construction. Thus the volume distribution can be used since it is less prone to numerical instabilities than the size distribution $n(r, a)$. We can write this with the spheroidal efficiencies Q_j from the scattering database for spheroidal particles [7], refractive index m

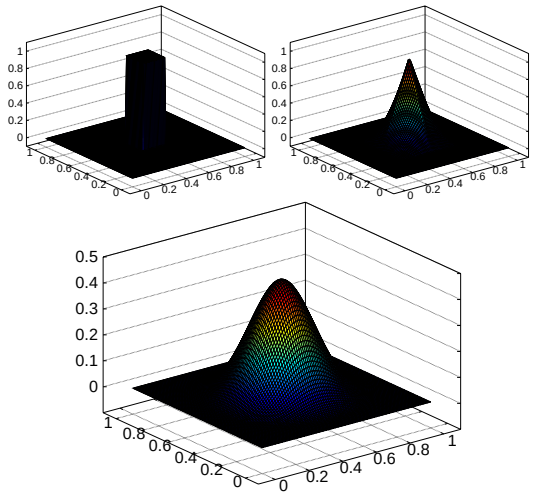

Figure 2: Some particular two-dimensional B-spline surfaces of orders 1, 2 and 4.

and surface S as

$$\Gamma_j(\lambda) = \int_{a_{\min}}^{a_{\max}} \int_{r_{\min}}^{r_{\max}} \frac{3S}{16\pi r^3} Q_j(r, \lambda, m, a) v(r, a) \mathrm{d}r\mathrm{d}a. \tag{2}$$

Thus, the integral over the size parameter is integrated again over a parameter representing the different aspect ratios. This means that we are here looking at 2D distributions, for more details see [8]. In contrast to [9] we do not use a particular separation product statement $v(r, a) = v_1(r)v_2(a)$. The retrieving problem of the distribution from the 2D Fredholm system of first kind Eq. 2 is ill-posed in nature and, therefore, needs particular regularization methods.

In the first step, for the discretization of Eq. 2 by collocation, one needs an extension of B-splines to two dimensions which are called the *B-spline surfaces* [10]. Instead of one, one has now two vectors of knots, one for each dimension. For illustration, see Fig. 2. In the second step, the resulting ill-conditioned linear equation system is solved by an iterative regularization technique, see [11] and [12].

2.1. Extinction efficiencies

First, we can find the effect, like for spheres, here that the efficiencies are smoother the larger the imaginary part of the refractive index becomes. Note how the differences in the optical efficiencies highly depend on the refractive index of the examined particles, see Fig. 3. For the non-absorbing case, $m = 1.5$, one can see a distinct ripple structure in the extinction efficiency. For the absorbing case with $m = 1.5 + 0.01\mathrm{i}$, however, this is not the case. Second, indeed, judging from that surface plot the extinction efficiency is more or less identical for all aspect ratios. This is a very important fact that we need to consider; it becomes apparent that the extinction efficiency,

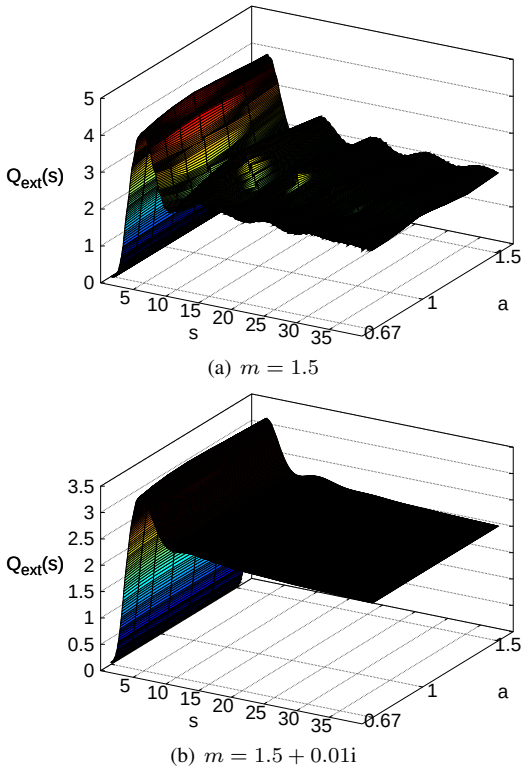

(a) $m = 1.5$

(b) $m = 1.5 + 0.01\mathrm{i}$

Figure 3: Spheroidal extinction efficiencies for two different refractive indices with $s = \pi r/\lambda$.

and thus the extinction coefficients, become independent of the particle shape for cases with higher absorption. For the inversion that means that the extinction data itself will not and cannot contain any viable information about the shape of the particles if the absorption is above a certain level.

2.2. Microphysical properties

We propose to extend the concept of microphysical properties to spheroidal particles, additionally integrating over the aspect ratio. Thus, we obtain the total surface-area concentration a_{t}, with G the geometrical cross-section,

$$a_{\mathrm{t}} = 4 \int_{a_{\min}}^{a_{\max}} \int_{r_{\min}}^{r_{\max}} G(r, a) n(r, a) \mathrm{d}r\mathrm{d}a \tag{3}$$

and the total volume concentration v_{t},

$$v_{\mathrm{t}} = \frac{4\pi}{3} \int_{a_{\min}}^{a_{\max}} \int_{r_{\min}}^{r_{\max}} r^3 n(r, a) \mathrm{d}r\mathrm{d}a, \tag{4}$$

while the effective radius is $r_{\mathrm{eff}} = 3\frac{v_{\mathrm{t}}}{a_{\mathrm{t}}}$. We will also introduce some new parameters to describe the variability with respect to the aspect ratio. For one, we will introduce the *mean aspect ratio*, defined by

$$\mu_a = \frac{\int_{a_{\min}}^{a_{\max}} a \int_{r_{\min}}^{r_{\max}} n(r, a) \mathrm{d}r\mathrm{d}a}{N_{\mathrm{t}}}, \tag{5}$$

as well as the *aspect ratio width*, which is defined by

$$\sigma_a = \frac{\int_{a_{\min}}^{a_{\max}} (a-\mu_a)^2 \int_{r_{\min}}^{r_{\max}} n(r,a)\mathrm{d}r\mathrm{d}a}{N_{\mathrm{t}}}, \qquad (6)$$

with $N_{\mathrm{t}} = \int_{a_{\min}}^{a_{\max}} \int_{r_{\min}}^{r_{\max}} n(r,a)\mathrm{d}r\mathrm{d}a$ the total number concentration. We have introduced these quantities as they will give us a good estimate as to the behavior of the 2D distribution with respect to the aspect ratio. As one can see, the mean aspect ratio μ_a is basically an estimate for the "central" aspect ratio of the distribution, while the aspect ratio width represents a value that describes how much the values deviate from the mean value. An important piece of data is the fraction of the total amount of the distribution that can be attributed to oblate and prolate spheroids and spheres. For that purpose, we introduce a parameter ξ, which describes a small deviation of the aspect ratio from the spherical value 1. Note that this does not mean we expect these particles to behave like spheres; it is instead used to introduce a measure for the retrieval of the particle shape. We set $\xi = 0.1$. The fraction quantities are given by

$$v^{\mathrm{sphere}} = \int_{1-\xi}^{1+\xi} \int_{r_{\min}}^{r_{\max}} v(r,a)\mathrm{d}r\mathrm{d}a/v_{\mathrm{t}}, \qquad (7)$$

$$v^{\mathrm{oblate(prolate)}} = \int_{a_{\min}(1+\xi)}^{1-\xi(a_{\max})} \int_{r_{\min}}^{r_{\max}} v(r,a)\mathrm{d}r\mathrm{d}a/v_{\mathrm{t}}. \qquad (8)$$

We have $v^{\mathrm{oblate}} + v^{\mathrm{sphere}} + v^{\mathrm{prolate}} = 1$. The $v^{\mathrm{particletype}}$ describes the fraction of the distribution that is made up of that particle type.

3. SIMULATION RESULTS

To test the validity of the proposed algorithm, we tested, firstly, it on data simulated with spherical particles. We have used data gained from the usual forward model assuming the (spherical) log-normal distribution with $r_{\mathrm{med}} = 0.1\mu\mathrm{m}, \sigma = 1.6, N_{\mathrm{t}} = 1$ with $m = 1.5 + 0.01\mathrm{i}$ at extinction wavelengths of 355 and 532 nm and backscatter wavelengths at 355, 532 and 1064 nm.

For the results, let us look at Fig. 4. We have performed the inversion without any error on the data. First, let us look at Fig. 4(b), 4(d) and 4(f), in which we have used the exact same forward data as in the spherical case. Interestingly, while the aspect-ratio-integrated distribution $v_a(r)$ in Figure 4(d) can be calculated quite exactly, the size-integrated distribution over the aspect ratios $v_r(a)$ as shown in 4(f) is very far from correct (of course, the true solution here just consists of a delta peak at $a = 1$).

For the other three figures on the left, Fig. 4(a), 4(c) and 4(e), we have also incorporated depolarization information. This means that in addition to the data points

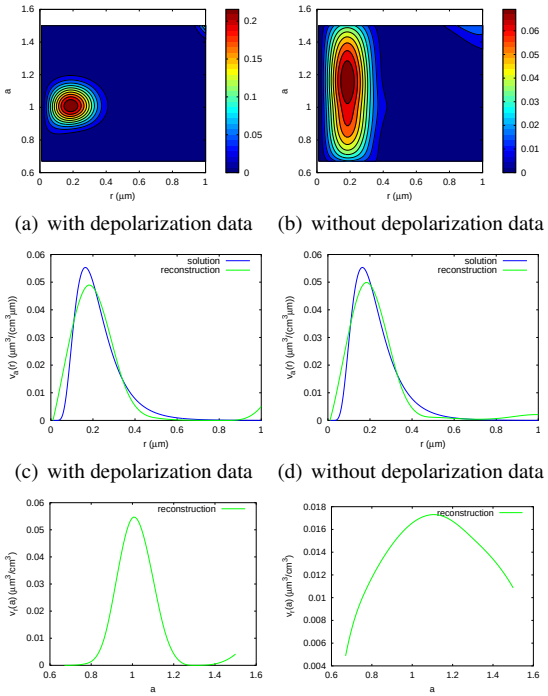

(a) with depolarization data (b) without depolarization data

(c) with depolarization data (d) without depolarization data

(e) with depolarization data (f) without depolarization data

Figure 4: Inverting data with the spheroidal model gained from a spherical forward model and a complex refractive index of $m = 1.5 + 0.01\mathrm{i}$. For (e) and (f), the exact solution consist of a delta peak at $a = 1$.

$355_{\mathrm{ext}}, 355_{\mathrm{bsca}}, 532_{\mathrm{ext}}, 532_{\mathrm{bsca}}$ and 1064_{bsca} we have included $355_{\mathrm{hv}} = 532_{\mathrm{hv}} = 1064_{\mathrm{hv}} = 0$, as we know that the simulated spherical particles will not result in any depolarized backscatter. As one can see from the figures, while the reconstruction of $v_a(r)$ is nearly identical, the reconstruction of $v_r(a)$ works much better here in this case. In Tab. 1, the reconstructions of the microphysical properties as defined in Eqs. 3-7 are given. Just as for spheres, the reconstruction of N_{t} still is problematic, while a_{t} and v_{t} can be reconstructed nearly perfectly both including and excluding depolarization data. The quality is different for μ_a and σ_a and the $v^{\mathrm{particletype}}$ properties, though. These quantities can be only reconstructed when the depolarization wavelengths are considered as one would expect.

This leads to a very interesting proposition, which we will further investigate in other examples; while information about the sizes of the particles are mostly included in the extinction and total backscatter data, the shape of the particles (here represented by the aspect ratio) can only be reliably determined with knowledge about the depolarization.

Secondly, we made quite a lot sensitivity studies with numerical simulations under different points of view. We show only one aspect here in using a prolate ensemble, for more details see [8]. Since the degree of ill-posedness is higher for spheroidal particles, see [8], more a-priori information is useful and very often necessary during

Table 1: Two-dimensional distribution retrieval with the spherical forward model and the spheroidal backward model.

property	exact value	retrieval with hv	retrieval without hv
r_{eff}	0.17	0.16	0.16
N_t	1	3.4	3.8
a_t	0.2	0.22	0.22
v_t	0.011	0.011	0.011
v^{oblate}	0%	8%	21%
v^{sphere}	100%	76%	28%
v^{prolate}	0%	16%	51%
μ_a	1	1.01	1.13
σ_a	0	0.083	0.35

Table 2: Reconstruction errors for the 2D case with a prolate ensemble. The numbers are the mean reconstruction errors for 100 error runs. The columns 2-4 and 5-7 show the reconstruction quality with and without depolarization data, respectively.

error level	1%	5%	15%	1%	5%	15%
r_{eff}	5%	7%	22%	5%	7%	24%
v_t	3%	4%	12%	5%	7%	22%
μ_a	6%	10%	23%	20%	23%	25%

the inversion process, here we use three depolarization profiles additionally to compare this effect as mentioned above. Whereas the effective radius is not influenced so much, it is the case for v_{t} and in particular for μ_a, see Tab. 2.

4. SUMMARY

In this work, a model used for forward calculation and inversion of aerosol optical properties that is based on Mie theory and used for spheres has been extended to work on spheroids, where the underlying kernel functions were exchanged by database values that have been calculated via a T-matrix method. We investigated a new 2D model to retrieve microphysical properties from optical Raman lidar and, additionally, depolarization data for non-spherical particles. From a mathematical point of view the problem is more ill-posed than for spherical particles. We found, retrieving non-spherical 2D particle distributions without using depolarization data fails more or less. Depolarization profiles are very valuable and urgently necessary, in particular, if prolate particles are present.

ACKNOWLEDGMENTS

This work was supported by the European Union seventh framework program Marie-Curie actions through ITARS project 289923.

REFERENCES

1. M. Mishchenko, L. Travis, and A. Lacis, *Scattering, Absorption, and Emission of Light by Small Particles*, NASA Goddard Institute for Space Studies, New York, 2005.

2. T. Rother, *Electromagnetic Wave Scattering on Nonspherical Particles: Basic Methodology and Simulations*, Springer, New York, 2009.

3. J. Gasteiger, S. Groß, V. Freudenthaler, and M. Wiegner, "Volcanic ash from Iceland over Munich: mass concentration retrieved from ground-based remote sensing measurements," *Atmos. Chem. Phys.*, vol. 11, pp. 2209–2223, 2011.

4. S. Otto, E. Bierwirth, B. Weinzierl, K. Kandler, M. Esselborn, M. Tesche, A. Schladitz, M. Wendisch, and T. Trautmann, "Solar radiative effects of a Saharan dust plume observed during SAMUM assuming spheroidal model particles," *Tellus B*, vol. 61, no. 1, pp. 270–296, 2008.

5. S. Otto, *Optische Eigenschaften nichtkugelförmiger Saharamineralstaubpartikel und deren Einfluss auf den Strahlungstransport in der Erdatmosphäre*, Ph.D. thesis, Leipzig University, 2012.

6. O. Dubovik, A. Sinyuk, T. Lapyonok, B. Holben, M. Mishchenko, P. Yang, T. Eck, H. Volten, O. Munoz, B. Veihelmann, W. van der Zande, J.-F. Leon, M. Sorokin, and I. Slutsker, "Application of spheroid models to account for aerosol particle nonsphericity in remote sensing of desert dust," *J. Geophys. Res.*, vol. 111, no. D11208, 2006.

7. K. Schmidt, J. Wauer, T. Rother, and T. Trautmann, "Scattering database for spheroidal particles," *Appl. Opt.*, vol. 48, no. 11, pp. 2154–2164, 2009.

8. L. Osterloh, *Retrieving Aerosol Microphysical Properties from Multiwavelength Lidar Data*, Ph.D. thesis, Potsdam University, 2011.

9. I. Veselovskii, O. Dubovik, A. Kolgotin, T. Lapyonok, P. Di Girolamo, D. Summa, D.H. Whiteman, M. Mishchenko, and D. Tanr, "Application of randomly oriented spheroids for retrieval of dust particle parameters from multi-wavelength lidar measurements," *J. Geophys. Res.*, vol. 115, no. D21203, pp. 10.1029/2010JD014139, 2010.

10. P. Deuflhard and A. Hohmann, *Numerical Analysis in Modern Scientific Computing. An Introduction*, Springer, New York, 2003.

11. L. Osterloh, C. Böckmann, R.E. Mamouri, and A. Papayannis, "An adaptive base point algorithm for the retrieval of aerosol microphysical properties," *The Open Atmos. Sci. J.*, vol. 5, pp. 61–73, 2011.

12. C. Böckmann and A. Kirsche, "Iterative regularization method for lidar remote sensing," *Comput. Phys. Commun.*, vol. 174, no. 8, pp. 607–615, 2006.